Soft Matter

PAPER

View Article Online
View Journal | View Issue

Cite this: *Soft Matter*, 2015, **11**, 1962

Solvent-dependent properties of poly(vinylidene fluoride) monolayers at the air–water interface†

Huie Zhu,[a] Jun Matsui,[b] Shunsuke Yamamoto,[a] Tokuji Miyashita[a] and Masaya Mitsuishi*[a]

Received 17th December 2014
Accepted 19th January 2015

DOI: 10.1039/c4sm02800g

www.rsc.org/softmatter

The present work addresses the solvent-dependent properties of Langmuir films of poly(vinylidene fluoride) (PVDF) and amphiphilic poly(*N*-dodecylacrylamide) (pDDA) at different mixing ratios. After introducing pDDA nanosheets, PVDF Langmuir films obtain a tremendously enhanced modulus as well as high transfer ratios using the vertical dipping method caused by the support of the pDDA two-dimensional hydrogen bonding network. Brewster angle microscopy (BAM) was used to investigate PVDF monolayers at the air–water interface *in situ*. Spreading from different solvents, the PVDF molecules take completely different aggregation states at the air–water interface. The PVDF molecules aggregate to become large domains when spread from *N*-methyl-2-pyrrolidone (NMP). However, the volatile and low-polarity methylethyl ketone (MEK) made the PVDF molecules more dispersive on the water surface. This study also discovers a versatile crystallization control of PVDF homopolymer from complete β phase (NMP) to complete α phase (MEK) at the air–water interface, thereby eliciting useful information for further manipulation of film morphologies and film applications.

1. Introduction

Organic ferroelectrics, especially poly(vinylidene fluoride) (PVDF) (Fig. 1) and its copolymers have attracted much attention over the past two decades because of their great potential in various applications such as energy storage, non-volatile memories, and sensors.[1–8] Semicrystalline PVDF and its copolymers generally include several crystallized phases such as a nonpolar α crystal, a polar β crystal, a partially polar γ crystal, a partially polar δ crystal, and a nonpolar ε crystal.[9–13] For various applications, polar β crystals are of critical importance because they show ferroelectric properties. Although many researchers have exerted great efforts to prepare PVDF-based ferroelectric devices, challenges remain in this research field. Particularly, their high voltage operation confines their further development. One effective method to resolve this problem is to fabricate an ultrathin ferroelectric film. However, ultrathin PVDF-based polymer films fabricated using spin-cast method were found with an extreme decrease in β crystal content and crystallinity, as well as a reduction in remanent polarization.[14] Ducharme *et al.* overcame this problem using Langmuir–Schafer (LS) technique to prepare poly(vinylidene fluoride-*co*-trifluoroethylene) (P(VDF-TrFE)) ultrathin films through horizontal deposition from the air–water interface. They demonstrated that no so-called threshold thickness exists for the crystallization of polymer ferroelectric films. Films as thin as two monolayers (about 1 nm) are ferroelectric, rather groundbreaking, and crucial for fabricating high-performance devices.[15,16] The ferroelectric LS films have been reported with a very high crystallinity and highly oriented structure with the polarization axis perpendicular to the film plane after thermal annealing treatment.[17]

Homopolymer PVDF has a lower crystallinity than PVDF copolymers have.[18] Considering that the Langmuir–Blodgett (LB) technique is an efficient process to construct well-organized and highly oriented uniform films at the air–water interface, it is expected to manipulate the orientation of PVDF homopolymer at the air–water interface using LB technique, thereby leading to high-content ferroelectric phases and high

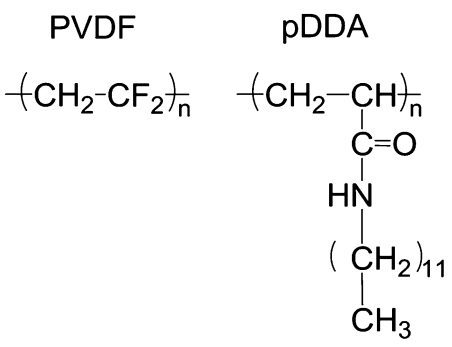

Fig. 1 Molecular structures of PVDF and pDDA.

[a]*Institute of Multidisciplinary Research for Advanced Materials (IMRAM), Tohoku University, 2-1-1 Katahira, Aoba-ku, Sendai 980-8577, Japan. E-mail: masaya@tagen.tohoku.ac.jp; Tel: +81-22-217-5637*

[b]*Department of Material and Biological Chemistry, Faculty of Science, Yamagata University, 1-4-12 Kojirakawamachi, Yamagata 990-8560, Japan*

† Electronic supplementary information (ESI) available. See DOI: 10.1039/c4sm02800g

crystallinity. However, seldom have reports described the preparation of PVDF homopolymer LB nanofilms, because of the unstable film-formation properties, although they promise higher dipole density and larger spontaneous polarization than copolymers. Chen *et al.* reported that PVDF homopolymer LS nanofilms were prepared using a horizontal deposition at a low surface pressure of 5 mN m^{-1}, which shows high ferroelectric phases after annealing at 135 °C.[19] However, the low transfer efficiency, necessary post-treatment (such as high-temperature annealing) and low compressibility are common disadvantages of the reported PVDF LS films using horizontal dipping deposition. We found recently that an amphiphilic polymer nanosheet of poly(*N*-dodecylacrylamide) (pDDA) (Fig. 1) was of immeasurable assistance to the stability and transfer ability of PVDF Langmuir film and "quasi-monolayers" at the air–water interface onto various substrates using a vertical deposition, as a result of the excellent hydrogen bonding network formed among pDDA molecules.[20] The as-prepared PVDF LB nanofilms with ultrahigh β crystal content show good ferroelectricity even for ultrathin films with thickness lower than 100 nm.[21] Excellent properties of the PVDF LB films must be related to the miscibility of PVDF and pDDA and the molecular interactions among them at the air–water interface. However, this has not been studied or reported in detail.[22] Particularly, the nucleation and crystallization at the ultrapure water surface are unique systems in comparison with other film preparation methods.[23] It is possible to uncover the mechanisms of domain formation, nucleation, and switching in the nanoscale at the air–water interface.[24]

In this study, solvent effects on the properties of PVDF Langmuir films at the air–water interface were demonstrated using two PVDF solutions: PVDF in *N*-methyl-2-pyrrolidone (*N*MP) and PVDF in methylethyl ketone (MEK). Polar solvents are typically used for PVDF solutions such as tetrahydrofuran (THF), acetone, MEK, dimethylformamide (DMF), and NMP, which are divisible into two categories: highly polar (DMF and NMP) and lowly polar (THF, acetone and MEK). We select NMP and MEK, respectively, as representatives for the two categories. NMP is a good solvent of PVDF with a polarity index (PI) of 6.7 (water is 10.2). MEK (PI = 4.7) has a lower polarity index than NMP and is a good swelling agent of PVDF at room temperature.[25] Two solutions show different interaction between the solvent and PVDF molecules.[26] The molecular aggregation states spread from different solvents were investigated by Brewster angle microscope (BAM) during compression. After introducing pDDA, the surface pressure (π)–area (A) isotherms of PVDF and pDDA mixtures were recorded at different mixing ratios, which demonstrate the miscibility of the two components. The film morphologies of different LB films were investigated using atomic force microscopy (AFM). The FTIR spectra were also characterized to investigate the pDDA hydrogen bonding network and the crystal structures in different PVDF–pDDA LB films.

2. Experimental section

2.1. Materials

PVDF ($M_n = 7.1 \times 10^4$, $M_w/M_n = 2.5$) was purchased from Aldrich, and used after reprecipitation. pDDA ($M_n = 3.0 \times 10^4$, $M_w/M_n = 3.0$) was synthesized through free radical polymerization initiated by 2,2′-azobisisobutyronitrile (AIBN) referring to the previous method.[27,28] The solvents NMP, DMF, acetone and chloroform were purchased from Wako Pure Chemical Industries Ltd. The solvent MEK were purchased from Tokyo Chemical Industry Co., Ltd. All solvents were used without further purification. Octyltrichlorosilane was purchased from Tokyo Chemical Industry Co. Ltd. for the substrate surface treatment.

2.2. π–A isotherm and BAM studies

Five kinds of solutions with concentration of 1 mM were prepared: PVDF in NMP, PVDF in DMF, PVDF in MEK, PVDF in acetone and pDDA in chloroform. To dissolve the polymer completely in MEK and acetone, respectively, we heated the systems at a temperature slightly lower than the boiling point (T_b), for instance at 70 °C for MEK (T_b = 80 °C) and 50 °C for acetone (T_b = 56 °C) for 1 h, respectively. Of these solutions, PVDF in DMF and PVDF in acetone are used as supporting information to enhance our results in the following discussion. The prepared solutions were spread onto the water surface in an automatically controlled Langmuir trough (FSD-220&21; U.S.I. Corp.) using a syringe to prepare Langmuir films. The subphase water was purified using an ultrapure water system (>17.5 MΩ cm, CPW-101; Advantec Toyo Kaisha Ltd.). To prepare a mixed monolayer of pDDA and PVDF, the pDDA solution was first spread with subsequent spreading of PVDF solution at different mixing ratios. After waiting for 30 min to remove the solvent completely (Fig. S1†), surface pressure (π)–area (A) isotherms were recorded at a compression rate of 10 mm min^{-1} at 20 °C. Brewster angle microscope (BAM) images (Mini BAM; KSV Nima) were obtained during isotherm measurements; the BAM images were taken using a CCD camera. The incident angle of the laser beam was fixed as the Brewster angle (53.1°) of the air–water interface, at which no light was reflected from the water surface. Therefore, the intensity of reflected light during compression depends solely on the Langmuir monolayer thickness.[29] The effective image size was 400 × 300 μm^2. The resolution was 2 μm^2.

2.3. Morphological studies and crystal structures of PVDF LB films

Silicon wafers were treated in a chloroform solution of octyltrichlorosilane for 3 h to obtain hydrophobic surfaces after ultrasonic and ozone cleaning. Langmuir films were transferred onto substrates using Langmuir–Blodgett (LB) or Langmuir–Schaefer (LS) technique. During deposition, the substrates were lifted at a constant dipping speed of 10 mm min^{-1} in both upstrokes and downstrokes. The morphologies of the obtained LB and LS nanofilms were investigated using atomic force microscopy (AFM) measurements conducted in tapping mode (SPA-400; Hitachi High-Tech Science Corp.). A silicon cantilever (14 nN m^{-1} and 132 kHz, Si-DF20; Hitachi High-Tech Science Corp.) was used. The Fourier transform infrared (FTIR) measurements were conducted at a spectral resolution of 4 cm^{-1} using an FTIR spectrometer (FTIR 4200; Jasco Corp.)

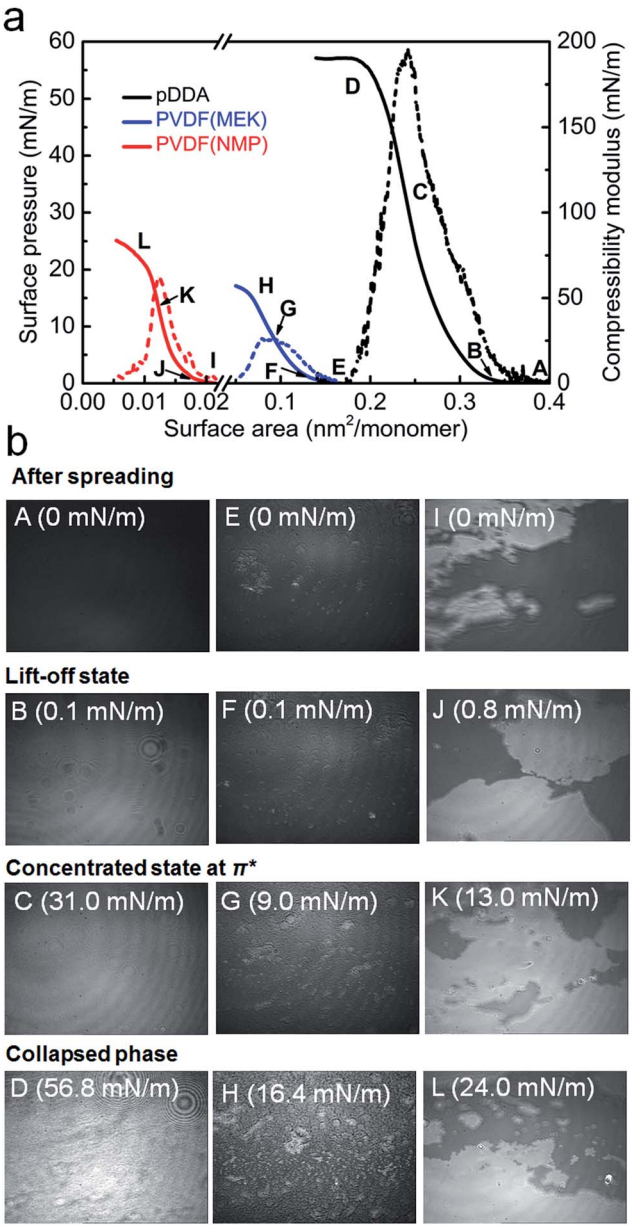

Fig. 2 (a) π–A isotherms of pDDA (black line) and PVDF spread from MEK (blue line) and NMP (red line) (solid lines), their corresponding compressibility modulus (dashed lines) and (b) BAM images at different surface pressures. Letters on the π–A isotherms correspond to those on BAM images, the values in brackets show surface pressures in respective states. The area of each image is 400 × 300 μm^2.

under a nitrogen atmosphere. All measurements were conducted at room temperature unless noted otherwise.

3. Results and discussion

3.1. Langmuir films of pure pDDA and PVDF

The polymer solutions were spread onto an air–water interface. Their π–A isotherms and BAM images were obtained at 20 °C. Fig. 2 shows the π–A isotherms of pure pDDA and pure PVDF spread from different solutions with BAM images at different surface pressures. Moreover, the compressibility modulus (or elasticity), C_s^{-1}, was calculated from isotherm data based on the following eqn (1) to obtain the monolayer elastic behavior as shown below.[23]

$$C_s^{-1} = -A(d\pi/dA) \quad (1)$$

In the C_s^{-1}–A curves in Fig. 2a, each compressed Langmuir film shows a peak value of C_s^{-1*}. The corresponding surface pressure and surface area at this state are designated respectively as π^* and A^*, which indicates the formation of a critical concentrated solid state.[30–33] In the whole compression process, polymer molecules pass through three regimes: a dilute regime in the initial state, a semidilute regime with the rapid increase of the compressibility modulus, and a concentrated regime (after the C_s^{-1*}).[30,31] In this state, collective entropic elasticity emerges.[31] High C_s^{-1} values correspond to low interfacial fluidity among the packed molecules in Langmuir films. A monolayer with a high C_s^{-1} value is rigid and difficult to deform.[32] The C_s^{-1*} of pure pDDA reaches 195.0 mN m^{-1} at $A^* = 0.24$ nm^2 per monomer (Table 1), which is ascribed to the excellent two-dimensional hydrogen bonding network formed in its monolayer at the air–water interface.[34] No report in the relevant literature has described $C_s^{-1*} > 190.0$ mN m^{-1} for polymer Langmuir films, although 82.4 and 150.0 mN m^{-1} have been reported, respectively, for poly(methylmethacrylate) (PMMA)[35] and the oligomer of p-phenylene vinylene.[36] At $A < 0.24$ nm^2 per monomer, the pDDA monolayer becomes concentrated and the modulus decreases to zero as a consequence of the strong decrease of the available free area at the air–water interface and of the conformational freedom degrees of polymer chains.[31,37,38] The BAM images in Fig. 2b(A–D) show that the pDDA monolayer behaviors with increasing surface pressure agree well with the isotherms: a dark homogeneous morphology at $\pi = 0$ mN m^{-1} (A), followed by a bright concentrated phase at $\pi^* = 31.0$ mN m^{-1} (C), corresponding to the formation of a compressed monolayer with homogeneous morphologies. The pDDA monolayer finally collapses at a very high collapse surface pressure (π_c) of 56.8 mN m^{-1}, which is indicative of its good film stability. However, PVDF Langmuir films spreading from MEK and NMP solutions show low C_s^{-1*} values of 26.4 and 62.8 mN m^{-1}, respectively corresponding to π^* of 9.0 and 13.0 mN m^{-1}, which indicates weak interaction between PVDF molecules, thereby leading to the low stability of the Langmuir films. Interestingly different BAM images were demonstrated for PVDF Langmuir films from different spreading solvents. In the case of PVDF(MEK), Fig. 2b(E) shows a dark image with small circular domains, which were surrounded by uniform reflected area even before compression at $\pi = 0$ mN m^{-1}.[39] Upon compression to $\pi = 0.1$ mN m^{-1} ($A = 0.14$ nm^2 per monomer) a lift-off state was generated at the air–water interface, from which the surface pressure starts to increase. In Fig. 2b(F), the compressed monolayer at $\pi^* = 9.0$ mN m^{-1} shows homogeneous morphology with a few aggregates. However, immediately after spreading the PVDF(NMP) solution onto the water surface, large domains with clearly defined edges were formed from the BAM images in Fig. 2b(I).[40] The BAM

Table 1 C_s^{-1} peak values at different mixing ratios and their corresponding surface areas and surface pressures[a]

PVDF(NMP) : pDDA	0 : 1	1 : 4	1 : 1	4 : 1	8 : 1	50 : 1	1 : 0
C_s^{-1*} (mN m^{-1})	195.0	173.1	154.0	150.0	142.0	136.0	62.8
A^* (nm^2 per monomer)	0.24	0.24	0.15	0.065	0.046	0.019	0.012
π^* (mN m^{-1})	31.0	26.6	26.6	26.8	26.0	28.3	13.0
π_c (mN m^{-1})	57.0	47.7	47.8	47.3	44.8	44.4	24.0

[a] C_s^{-1*} is the peak compressibility modulus with the corresponding surface pressure and area of π^* and A^*, respectively. π_c denotes the collapsed surface pressure.

images show that PVDF molecules do not form a gas analogous phase. The PVDF molecules exist as multilayers in the domains at the air–water interface.[20,41] The different solubility of MEK and NMP in water might engender different aggregation states of PVDF molecules at the air–water interface. MEK has solubility of 27.5 g in 100 mL water, whereas NMP has greater solubility, up to 100 g/100 mL. Results show that NMP molecules dissolved rapidly in water, which makes PVDF domains remain at the air–water interface without sufficient dispersion, as distinct from PVDF spread from MEK. This rapidity shows good agreement with the difference of the limiting surface area between these two cases. By extrapolating the linear portion of the condensed state in the π–A isotherms to zero,[42] the limiting surface areas of VDF repeating units were ascertained as 0.12 and 0.015 nm^2, respectively, for PVDF(MEK) and PVDF(NMP) Langmuir films. The occupied area per VDF unit from MEK is about seven times more dispersive than that from NMP at the air–water interface. The C_s^{-1}–A isotherm of PVDF(NMP) Langmuir film showed a small shoulder at A = 0.017 nm^2 per monomer before C_s^{-1*}, indicating a monolayer phase transition. This phase transition took place because the domains were brought into contact.[35,40] We infer that PVDF molecules in the PVDF Langmuir films of two kinds occupy the area with different molecular conformations. Therefore, changing solvent properties is effective to modulate molecular aggregation of PVDF at the air–water interface. The information related to crystalline phases of two kinds of PVDF Langmuir films will be discussed later using FTIR measurements.

3.2. PVDF(NMP)–pDDA Langmuir films at different mixing ratios

A previous work revealed that a tiny amount of pDDA was effective to improve the PVDF(NMP) Langmuir film properties, including the stability at the air–water interface and the transfer ability onto substrates.[20] In Fig. 3a, the π–A isotherms of PVDF(NMP) and pDDA mixtures at different molar ratios from 1 : 4 to 50 : 1 show a series of steep curves with high collapse surface pressure (π_c > 40 mN m^{-1}). Miscibility of components in a mixed monolayer can be estimated by analyzing the π–A isotherms. If the components are immiscible, then two collapse states are observed, corresponding to the pure components.[22] A consecutive increase with a steep slope in the π–A isotherms shows that two components in this system are not phase separation. The π–A isotherms of PVDF(DMF)–pDDA have similar consecutive increase and improved collapse surface pressure after introducing pDDA component as shown in Fig. S2.† The corresponding C_s^{-1}–A isotherms of PVDF(NMP)–pDDA Langmuir films are portrayed in Fig. 3b. The mixtures qualitatively show behaviors between the extremes of pDDA and PVDF with higher C_s^{-1*} values than that of pure PVDF. Even at the mixing ratio of 50 : 1, the value of the C_s^{-1*} is much higher than that of pure PVDF(NMP), 62.8 mN m^{-1}, because of the presence of the pDDA hydrogen bonding network. The C_s^{-1} peak values decreased from 173.1 to 136.0 mN m^{-1} with the increase of mixing ratios from 1 : 4 to 50 : 1 (Table 1), indicating that the integrity of the hydrogen bonding network between pDDA

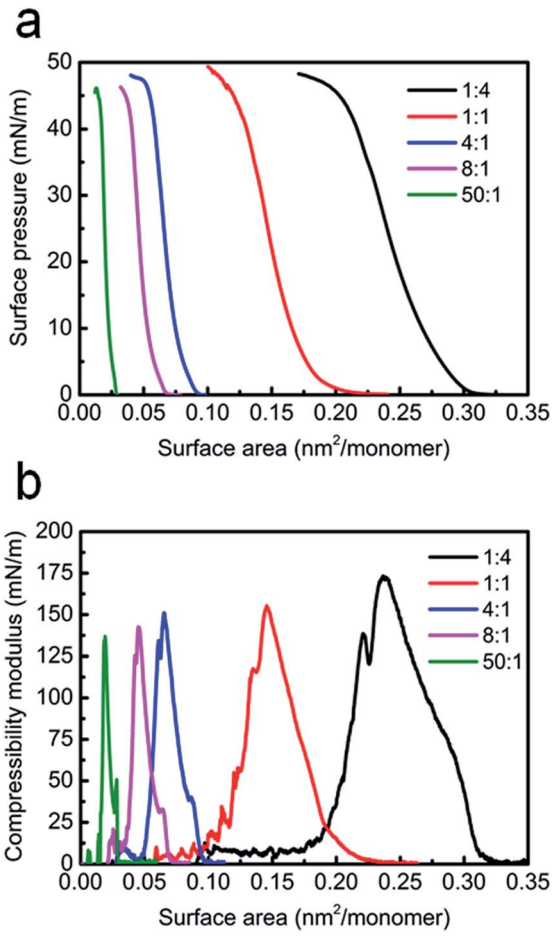

Fig. 3 (a) π–A isotherms and (b) the corresponding C_s^{-1}–A isotherms of PVDF(NMP)–pDDA Langmuir films at different molar mixing ratios (PVDF : pDDA): 1 : 4 (black line), 1 : 1 (red line), 4 : 1 (blue line), 8 : 1 (pink line), and 50 : 1 (green line).

molecules was disturbed slightly by the PVDF domains. The BAM images in Fig. S3† show images of the floating mixed monolayers. In the initial dilute regime ($\pi = 0$ mN m^{-1}), PVDF and pDDA mixtures showed oil circles with PVDF solid domains in Fig. S3a.† After compression, films change from a semidilute regime to a critical concentrated state (Fig. S3b†). Further compression eventually led to the monolayers' collapse (Fig. S3c†), corresponding to a sharp decrease of C_s^{-1} in the C_s^{-1}–A isotherms. This results from the strong reduction of the available free area at the air–water interface and of the conformational freedom degrees of polymer chains.[31] The small peaks appearing in the C_s^{-1}–A isotherms after the $C_s^{-1^*}$ peaks result from the intrinsic properties of pDDA Langmuir films because all the corresponding surface pressures are almost identical, as shown in Table S1.† No such peaks are observed for 50 : 1 or pure PVDF.

Fig. 4 shows BAM images of the PVDF(NMP)–pDDA Langmuir film at 50 : 1. PVDF forms domains such as the pure PVDF(NMP) Langmuir film once spread onto the water surface (Fig. 4a). Compression brings the domains mutually closer (Fig. 4c and d). In comparison with the pure PVDF(NMP) Langmuir film (Fig. 2b), the dark area among the PVDF domains in the BAM images is occupied by pDDA monolayers, which can form a two-dimensional hydrogen bonding network. Such a network confined the PVDF domains. Therefore, there exists some interaction between the PVDF domain boundaries and the pDDA monolayer, such as the hydrogen bonding interaction. The existence of the hydrogen bonding interaction can be confirmed by the shift of N–H vibration modes of pDDA toward a lower wavenumber in FTIR spectra as shown in Fig. S4a,† likewise what happened in the case of the addition of PMMA into PVDF matrix.[43,44] We also found that the vibration modes of $\nu_s(CH_2)$, $\nu_a(CH_2)$, and $\nu_a(CH_3)$ in pDDA shift respectively from 2850 to 2854 cm^{-1}, from 2920 to 2925 cm^{-1}, and from 2955 to 2962 cm^{-1} with the increasing mixing ratio of PVDF : pDDA, as shown in Fig. S4b.†[45] This shift is characteristic of slightly increasing disorder of the pDDA monolayer with increasing PVDF content in PVDF–pDDA Langmuir films due to the fewer opportunities for van der Waals interactions among adjacent DDA units,[46] which is in accord with the decrease of $C_s^{-1^*}$ values in Fig. 3b.

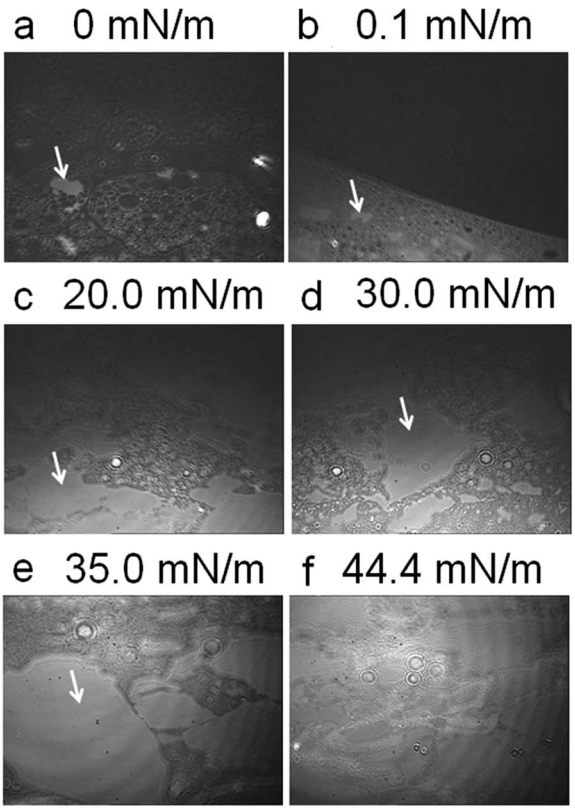

Fig. 4 BAM images for PVDF(NMP)–pDDA Langmuir films at 50 : 1 at different surface pressures: (a) 0 (after spreading), (b) 0.1 (lift-off state), (c) 20.0, (d) 30.0 (π^*), (e) 35.0, and (f) 44.4 mN m^{-1} (collapsed phase). (PVDF domains are marked by the white arrows. The area of each image is 400 × 300 μm^2).

3.3. PVDF(MEK)–pDDA Langmuir films at different mixing ratios

Fig. 5a shows the π–A isotherms of the mixtures of PVDF(MEK) and pDDA at different mixing ratios at 20 °C. The isotherm shape changed with the increasing mixing ratios. The π–A isotherms are classifiable into three categories: pDDA-rich (1 : 4, 1 : 1), PVDF-rich (4 : 1, 8 : 1), and PVDF-overmuch (50 : 1) Langmuir films. First, when pDDA was rich, the isotherms showed similarly steep curves to that of pDDA, shifting the limiting surface area to smaller values of 0.27 (1 : 4) and 0.23 (1 : 1) nm^2 per monomer. Furthermore, their collapse surface pressures (π_c) were lowered respectively to 38.5 and 36.1 mN m^{-1} in comparison with that of pure pDDA, 57.0 mN m^{-1}, as shown in Table 2. With the increasing content of PVDF above 4 : 1, two-plateau curves emerged with both the typical plateaus of PVDF(MEK) and the following steep curve corresponding to pDDA solid monolayers in the π–A isotherms. The two collapse stages clearly indicate phase separation because of immiscibility of the two components.[22] Similarly, spread from acetone, the PVDF–pDDA Langmuir films also show phase separation by the two-plateau curves in Fig. S5.† Therefore, it is reasonable that we selected NMP and MEK, representatively as previously discussed.

The corresponding C_s^{-1}–A isotherms in Fig. 5b clearly show two peaks for PVDF-rich Langmuir films (4 : 1 and 8 : 1), also indicating that the two components are immiscible when PVDF is spread from the MEK solution. The values of the peak compressibility modulus, the corresponding surface pressure and the surface area are presented in Table 2. The collapse surface pressure (π_c) was decreased with increasing mixing ratios. BAM images of PVDF(MEK)–pDDA Langmuir films at different mixing ratios from 1 : 4 to 8 : 1 are shown in Fig. 6. All the PVDF(MEK)–pDDA Langmuir films at different mixing ratios from 1 : 4 to 8 : 1 have similar compression behaviors. During compression, the monolayer behaviors consisted of several stages. At $\pi = 0$ mN m^{-1}, a dilute state is visible in Fig. 6a.[30] Both PVDF and pDDA coexisted at the interface at low surface pressures before the first peak value of $C_s^{-1^*}$ with homogeneous morphologies in Fig. 6b.[47] The first collapse

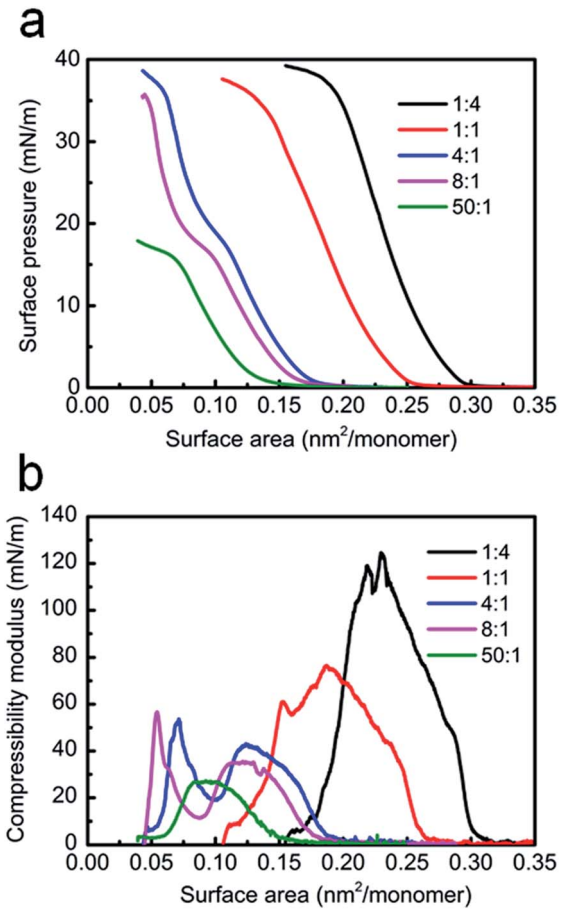

Fig. 5 (a) π–A isotherms and (b) the corresponding C_s^{-1}–A isotherms of PVDF(MEK)–pDDA Langmuir films at different molar mixing ratios (PVDF : pDDA): 1 : 4 (black line), 1 : 1 (red line), 4 : 1 (blue line), 8 : 1 (pink line), and 50 : 1 (green line).

Table 2 C_s^{-1} peak values at different mixing ratios and their corresponding surface area and surface pressures and the collapse surface pressures[a]

PVDF(MEK) : pDDA	1 : 4	1 : 1	4 : 1	8 : 1	50 : 1
C_s^{-1*} (mN m^{-1})	125.0	77.4	43.0	35.5	27.2
A^* (nm^2 per monomer)	0.23	0.19	0.12	0.12	0.093
π^* (mN m^{-1})	18.0	17.0	12.2	9.8	8.6
C_s^{-1**} (mN m^{-1})	119.5	61.3	53.8	57.1	–
A^{**} (nm^2 per monomer)	0.22	0.15	0.071	0.054	–
π^* (mN m^{-1})	26.0	30.0	28.6	29.8	–
π_c (mN m^{-1})	38.5	35.9	36.1	35.2	16.4

[a] C_s^{-1*} and C_s^{-1**} respectively denote the peak values of the compressibility modulus at the first and second peaks with the surface areas of A^* and A^{**}. π^* and π^{**} are the corresponding surface pressures. π_c is the collapse surface pressure.

plateau at π = 17.0 mN m^{-1} in the π–A isotherms (Fig. 5a) corresponds to the composition-dependent collapse of PVDF for 4 : 1 and 8 : 1.[48] With further compression to the second peak of the compressibility modulus (C_s^{-1**}), PVDF molecules were extruded out of the interface to form small domains indicated by the white arrows, as seen from the BAM images (Fig. 6c), which indicates that the two components are immiscible even in the pDDA-rich cases, although two-plateau curves were not observed in the π–A isotherms of PVDF(MEK)–pDDA Langmuir films at 1 : 4 and 1 : 1. With the increasing content of PVDF, the number of these domains increases. Subsequent compression produced the dense pDDA two-dimensional monolayers, constructed on account of the pDDA hydrogen bonding networks. At π_c in Table 2, such hydrogen bonding networks were broken. More domains came out in the BAM images accompanying the film collapse (Fig. 6d).

When the content of PVDF exceed that of pDDA significantly at the mixing ratio of 50 : 1, however, a low π_c was obtained because 16.4 mN m^{-1} was caused by the negligible effect of the tiny pDDA on the well dispersed PVDF molecules during compression, completely differing from the phenomenon in the case of PVDF(NMP) : pDDA = 50 : 1. The small size of our Langmuir trough limited the possibility of detecting the second collapse: the steep curve for the pDDA monolayer.[49] The BAM images presented in Fig. S6† show the monolayer behaviors of PVDF(MEK)–pDDA Langmuir film at 50 : 1, similar to those of pure PVDF(MEK). The average limiting surface area (S_{aver}) is attained by extrapolating the linear portion of the condensed state in the π–A isotherms to zero. The limiting surface area per DDA repeating unit (S_{DDA}) is 0.28 nm^2, in good agreement with the reported value.[20] Then the limiting surface area per VDF repeating unit (S_{VDF}) at the air–water interface was calculated using $S_{aver} = S^*_{VDF}x + S^*_{DDA}(1 - x)$, where x denotes the molar content of VDF repeating units.[20,50] The S_{aver} for PVDF(NMP)–pDDA and PVDF(MEK)–pDDA Langmuir films at 50 : 1 are, respectively, 0.024 and 0.12 nm^2. The S_{VDF} value for PVDF(NMP)–pDDA and PVDF(MEK)–pDDA Langmuir films at 50 : 1 is calculated, respectively, as 0.0190 and 0.117 nm^2. Consequently, the specific area of PVDF in both cases was obtained as 77.6% and 97.5%, respectively, which are consistent with the BAM images in Fig. 4e and S6d,† respectively. This fact also indicates that PVDF(MEK)–pDDA Langmuir films at 50 : 1 behavior is similar to that of the pure PVDF(MEK).

3.4. Deposition and morphological studies of PVDF–pDDA LB films

For comparison, we first tried to transfer pure PVDF(NMP) and PVDF(MEK) Langmuir films onto substrates using LS method (see ESI†). Detachment occurred during deposition. Therefore, the Langmuir films have very low transfer ratios of less than 0.30, as shown in AFM images of their monolayers (Fig. S7†). For effectively transferring the PVDF Langmuir films, we examined the PVDF-rich Langmuir films. The PVDF(NMP)–pDDA Langmuir films at 50 : 1 were transferred onto a hydrophobic silicon substrate by the vertical deposition method at π = 30.0 mN m^{-1}. The transfer ratios for upstrokes and downstrokes were almost unity up to at least 100 layers, which is in accordance with the previous report. Between PVDF multilayer domains, the continuous pDDA hydrogen bonding network supports the formation of stable PVDF–pDDA Langmuir film and affords them the transfer ability, as discussed previously. For effectively depositing PVDF(MEK)–pDDA Langmuir films,

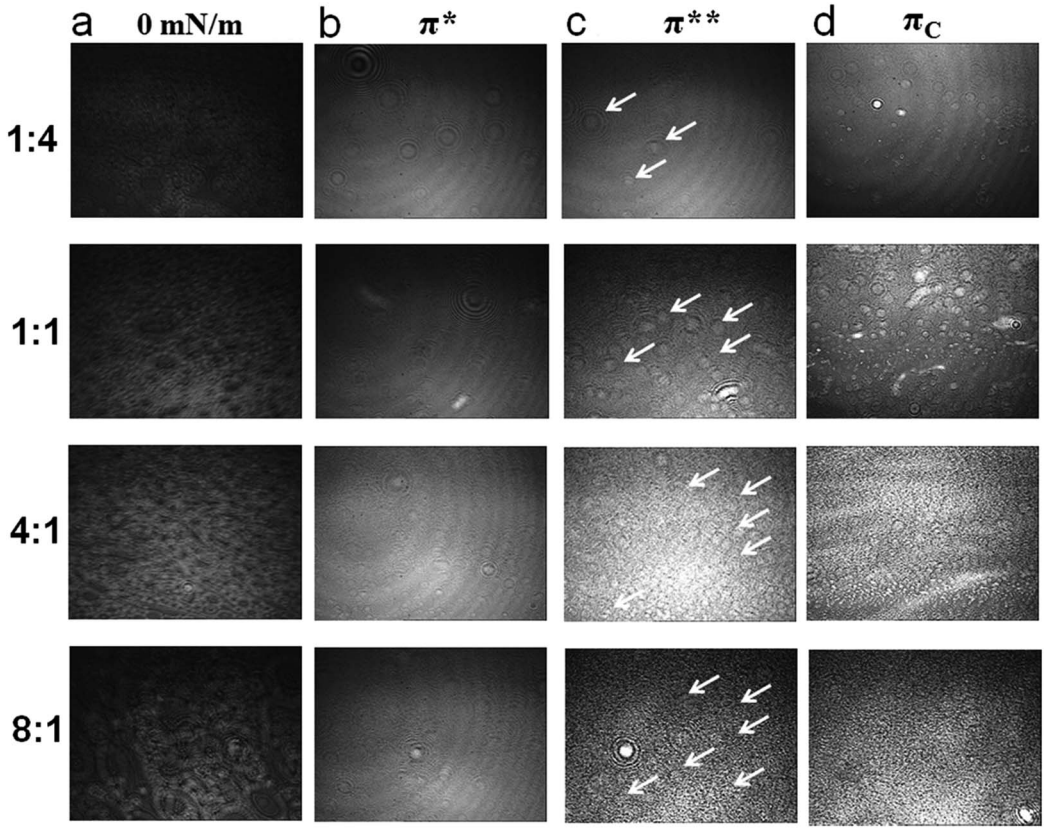

Fig. 6 BAM images of PVDF(MEK)–pDDA Langmuir films at different surface pressures: (a) 0 mN m^{-1} (right after spreading), (b) π*, (c) π**, and (d) the collapsed phase (π_c). The area of each image is 400 × 300 μm^2.

we selected the mixing ratio at PVDF(MEK) : pDDA = 8 : 1, not only because of the higher collapse surface pressure, but also because of the PVDF-rich properties. The Langmuir films were transferred successfully onto hydrophobic silicon substrates at π = 30.0 mN m^{-1} with a unity transfer ratio for both upstrokes and downstrokes. However, at π = 9.0 mN m^{-1}, the transfer efficiency is as low as 0.35. This result demonstrates that a higher surface pressure for the deposition of PVDF(MEK)–pDDA Langmuir films is more effective. We consider that a higher surface pressure is necessary for the formation of the pDDA hydrogen bonding network. In the case of the PVDF(MEK)–pDDA Langmuir film at 50 : 1, the film transfer was just made in downstrokes to form X-type structures. The transfer ratio at the first cycle was unity. Nevertheless, it decreased with increasing deposition cycles. At the first ten cycles, the average value of the transfer ratio for downstrokes was about 0.78 onto the hydrophobic silicon substrates. Detachment was observed during film deposition. It becomes less than 0.30 after 20 cycles, which also indicates that the low collapse surface pressure might not allow the formation of the pDDA hydrogen bonding network, which is expected to be of great importance for transferring PVDF Langmuir films.

Fig. 7 portrays AFM images of PVDF–pDDA LB monolayers from PVDF(NMP)–pDDA Langmuir film at 50 : 1 and PVDF(MEK)–pDDA Langmuir film at 8 : 1. The PVDF(NMP)–pDDA Langmuir film is very stable after reaching the set surface pressure. However, the PVDF(MEK)–pDDA Langmuir film has worse stability accompanying a decreasing surface area as time passes. The PVDF(NMP)–pDDA LB monolayer in Fig. 7a shows a smooth surface with thickness of about 2.27 nm, which is in good agreement with our previous report of about 2.31 nm per monolayer.[20] Fig. 7b and c respectively show PVDF(MEK)–pDDA LB monolayers deposited at 30.0 and 9.0 mN m^{-1}. The diamond-shape structures appear in both cases with regular size. These microstructures are apparently α single crystals because they have been reported as diamond shapes.[51] The sizes of the

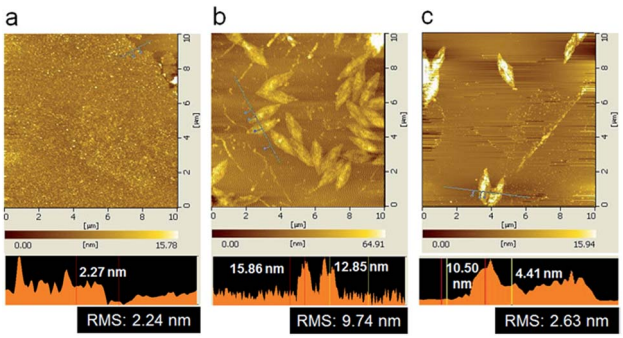

Fig. 7 AFM images of LB monolayers on the hydrophilic silicon substrates (a) PVDF(NMP) : pDDA = 50 : 1 deposited at 30.0 mN m^{-1}, (b) PVDF(MEK) : pDDA = 8 : 1 deposited at 30.0 mN m^{-1} and (c) PVDF(MEK) : pDDA = 8 : 1 deposited at 9.0 mN m^{-1}.

diamonds in Fig. 7b and c are roughly equal: about 0.78 μm (short diagonal line) × 2 μm (long diagonal line). The microstructures in Fig. 7b have a larger number than that in Fig. 7c and a more homogeneous surface, which indicates that soft interface compression is extremely effective for microstructural growth. The decrease in the surface area observed during the constant surface pressure mode for the formation of PVDF(MEK)–pDDA Langmuir films might be attributable to the growth of such microstructures. AFM images of PVDF–pDDA LB films with multilayers are shown in Fig. S8.† Numerous fiber-like structures in the PVDF(NMP) represent high crystallinity (Fig. S8a†). The PVDF aggregates, however, form in the PVDF(MEK)–pDDA LB multilayer films, coming from the stacking of diamond-shaped microstructures (Fig. S8b and c†).

For confirming the functionality of the pDDA hydrogen bonding network on the transfer properties, we measured the FTIR spectra of the PVDF–pDDA LB films deposited at 30.0 mN m^{-1} (Fig. 8). Coleman *et al.* reported that the vibration modes at 3447 and 3300 cm^{-1} are assigned respectively to the N–H stretching modes of the "free" and hydrogen bonded N–H groups of polyamide.[52] However, the carbonyl stretching region suggests the presence of at least three bands at 1638, 1656, and 1680 cm^{-1}, which are attributed respectively to the ordered and disordered hydrogen bonded carbonyl groups and the "free" carbonyl groups.[52] In Fig. 8a, both "free" and hydrogen bonded N–H groups are observed for the PVDF(NMP)–pDDA and PVDF(MEK)–pDDA LB films deposited at 30 mN m^{-1} because of the coexistence of the peaks at 3413 and 3294 cm^{-1}. Fig. 8b also shows that the LB films have "free" C=O stretching modes at 1689 and 1680 cm^{-1}, respectively. The high intensity of the hydrogen bonded N–H at 3294 cm^{-1} in comparison with the "free" N–H groups at 3413 cm^{-1} in the PVDF(NMP)–pDDA LB film demonstrates that hydrogen-bonded N–H groups have dominant interaction. The dominantly ordered hydrogen bond zone at 1639 cm^{-1} further proves the formation of the two-dimensional hydrogen bonding network of pDDA in the PVDF(NMP)–pDDA LB film as expected. In addition, the peak at 1663 cm^{-1} in the PVDF(NMP)–pDDA LB film is indicative of the existence of the random hydrogen bonding interaction, which is consistent with the results obtained from isotherms. The dominant signal of the hydrogen bonded N–H groups in the PVDF(MEK)–pDDA LB film was also observed. The higher fraction of ordered hydrogen-bonded zone at 1641 cm^{-1} than that of PVDF(NMP)–pDDA LB film results from the higher content of pDDA in the PVDF(MEK)–pDDA LB film. These ordered hydrogen bonding interactions correspond to the pDDA hydrogen bonding network in the PVDF–pDDA LB film. Such an interaction network is the very one to endow the transfer ability of the PVDF–pDDA Langmuir films. At a lower surface pressure of 9.0 mN m^{-1} (Fig. S9†), however, a large amount of "free" carbonyl groups at 1689 cm^{-1} in comparison with the film deposited at the higher surface pressure exists in PVDF(MEK)–pDDA LB films at 50 : 1. This large amount corresponds to the absence of the pDDA hydrogen bonding network, which results in the low transfer ability of the PVDF(MEK)–pDDA LB films at 50 : 1. The FTIR of PVDF(MEK)–pDDA LB films at 8 : 1 deposited at 9 mN m^{-1} presents similar results. Therefore, high surface pressure is necessary for the formation of the pDDA hydrogen bonding network and for the endowment of the transfer abilities of PVDF(MEK)–pDDA Langmuir films.

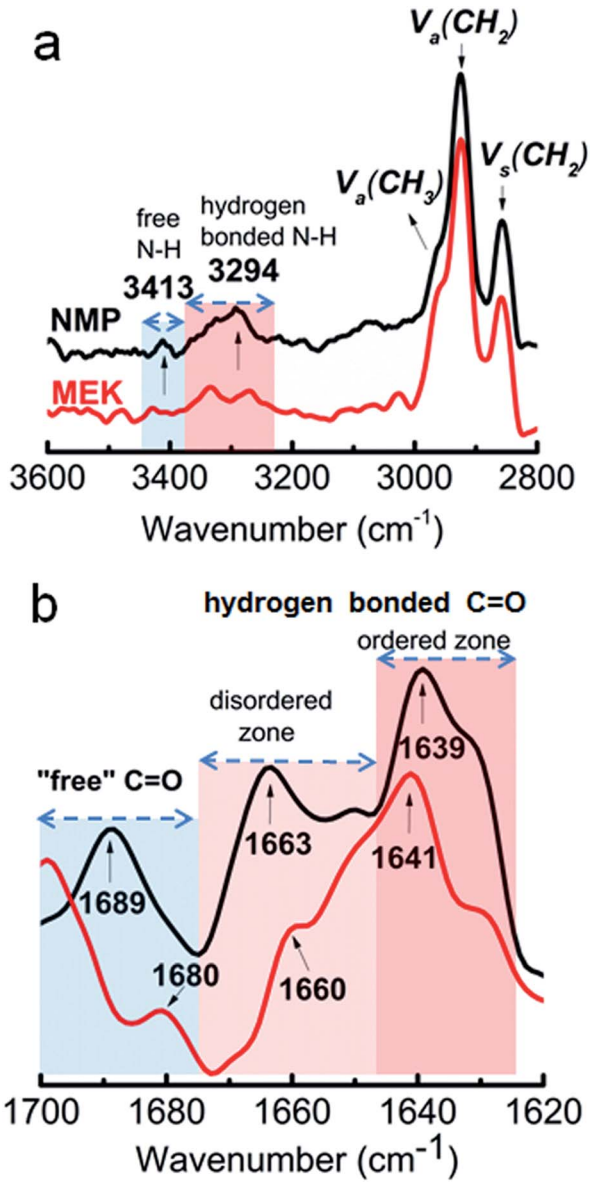

Fig. 8 FTIR spectra in the regions (a) 3600–2800 cm^{-1}, and (b) 1700–1620 cm^{-1} of 20-layer PVDF(NMP)–pDDA LB film at 50 : 1 (black line) and 20-layer PVDF(MEK)–pDDA LB film at 8 : 1 (red line) deposited at 30.0 mN m^{-1}.

3.5. Crystal structures of PVDF molecules in the PVDF–pDDA LB films

For the assignment of crystal structures of PVDF films, we investigated the FTIR spectra at the region of 1430–700 cm^{-1}, where the characteristic absorption of PVDF usually appears. As reported, well-known peaks at 763, 795, 976, and 1384 cm^{-1} are assigned to non-polar α crystals (Form II). The β crystal (Form I) is associated with absorptions at 840, 1276, and 1402 cm^{-1}, whereas the peak at 1233 cm^{-1} is characteristic for the γ crystal (Form III).[53–56] In addition, two other evident peaks at 878 and

1185 cm^{-1} originate from the rocking mode of CF_2.[57] As Fig. 9 shows, β crystals are dominant in PVDF(NMP)–pDDA LB films because of the sharp intensities of the Form I peaks. For PVDF(MEK)–pDDA LB films, a large content of α crystals appear with negligible β crystals. The relative fraction of β and α crystals for different films was calculated according to the reported eqn (2), assuming that only the two crystal forms can be found in the LB nanofilms.[58]

$$F(\alpha) = \frac{A_\alpha}{A_\alpha + \left(\frac{K_\alpha}{K_\beta}\right)A_\beta}, \; F(\beta) = \frac{A_\beta}{\left(\frac{K_\beta}{K_\alpha}\right)A_\alpha + A_\beta} \qquad (2)$$

Therein, A_α and A_β respectively represent the absorbance of α and β crystals at 763 and 840 cm^{-1}. K_α and K_β are the absorption coefficients at the respective wavenumbers of 6.1×10^4 and 7.7×10^4 cm^2 mol^{-1}. The $F(\beta)$ is calculated to be 95.9% in PVDF(NMP)–pDDA LB films, which is consistent with the reported value.[20] The $F(\alpha)$ is calculated to be 98.4% in PVDF(MEK)–pDDA LB films. We have already reported that higher surface pressure is more effective for obtaining higher content of PVDF β crystals in PVDF(NMP)–pDDA LB films. According to AFM images of the PVDF(NMP)–pDDA and PVDF(MEK)–pDDA LB films deposited at 30.0 mN m^{-1}, spreading solvent properties are critical for modulating the crystal structures and morphological properties in the obtained PVDF–pDDA LB films. Herein, we can also easily modulate the crystal phases from β-dominant to α-dominant in the nanoscale by changing spreading solvents. These are usually challenging points in this research field.

Salimi *et al.* reported that variations in the solvent polarity and ability can induce a specific conformation in polymer chains through changes in chain coil dimensions during the preparation of PVDF solution-cast films.[26] They also found that the intermolecular interactions between PVDF and *N*,*N*-dimethylacetamide (DMAc), a highly polar solvent are of critical

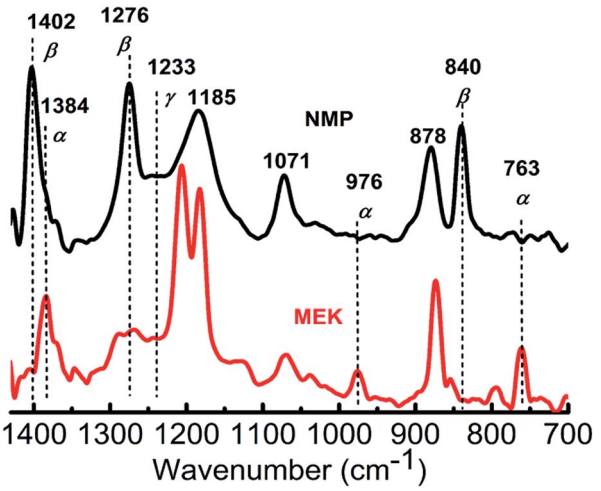

Fig. 9 FTIR spectra in the region of 1430–700 cm^{-1} of 20-layer PVDF(NMP)–pDDA LB film (black line) at 50 : 1 and 20-layer PVDF(MEK)–pDDA LB film (red line) at 8 : 1 deposited at 30.0 mN m^{-1}.

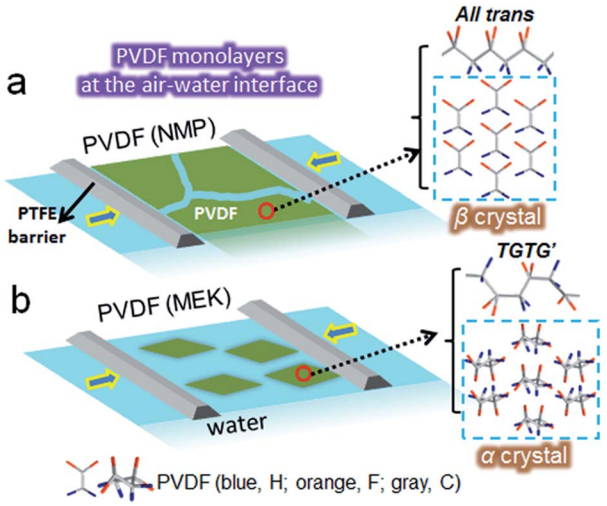

Fig. 10 Schematic illustration of PVDF chain conformations: (a) PVDF(NMP) and (b) PVDF(MEK) monolayers at the air–water interface.

importance to rotate the C–F bonds around C–C bonds to induce PVDF all-*trans* conformation during polymer crystallization in a low-temperature environment (<60 °C). The crystallization system at the air–water interface for PVDF(NMP) is also at a low temperature (20 °C). PVDF molecules at the air–water interface interacting with highly polar NMP molecules are likely to take a polarized and extended all-*trans* conformation by rotating the dipoles of C–F bonds in the PVDF molecular chains (Fig. 10a).[26,44] The extended and polarized PVDF(NMP) molecules are frozen, accompanying the fast dissolution of NMP into water, which results in the nucleus formation of PVDF β crystals. Surface compression facilitates the further growth of these crystals. This fact shows good agreement with the reported result that the content and the regularity of β crystals in the PVDF(NMP)–pDDA LB films is increased with the increasing surface pressure.[20] However, the polymer–solvent interaction in PVDF(MEK) system is not sufficiently strong to rotate the C–F bonds, which makes PVDF molecules take more coiled conformations at the air–water interface.[56] The non-solvent water for PVDF as well as the soft compression will impose a confinement effect on PVDF coiled chain diffusion and crystal growth, which facilitates the formation of α-phase PVDF with a *trans–gauche–trans–gauche* (TGTG′) molecular conformation (Fig. 10b).[26,59]

4. Conclusions

Using π (or C_s^{-1})–*A* isotherms and BAM images, this study examined the formation of various PVDF Langmuir films. The spreading solvents play a key role in the properties of PVDF Langmuir films at the air–water interface, as well as the crystal structures in the obtained PVDF–pDDA LB films. The PVDF(NMP) molecules at the air–water interface form scalable domains because of the high solubility of NMP in water. The PVDF(MEK) Langmuir film is uniform. A miniscule amount of pDDA is effective in enhancing the properties of PVDF(NMP)–pDDA Langmuir films on account of the ordered hydrogen bonding network formed among pDDA molecules. Such a hydrogen

bonding network is the very reason that the transfer ability was enhanced tremendously in the PVDF(NMP)–pDDA Langmuir films. However, phase separation in PVDF(MEK)–pDDA Langmuir films was found from the two-plateau π–A isotherms as well as the BAM images. This study provides valuable information related to the morphological evolution of semicrystalline PVDF confined in a pDDA two-dimensional geometry at the air–water interface and gives fundamental insight into the influence of solvents on the Langmuir film properties. In the case of PVDF(MEK)–pDDA LB films (8 : 1), soft compression is necessary to form regular diamond microstructures that are analogous to the PVDF α-single crystals, which will be studied further in the future. This study presents very interesting and controllable crystal structures in mixtures of nonamphiphilic PVDF and amphiphilic pDDA at the air–water interface, which are expected to afford much useful information for additional interface manipulation of PVDF crystals.

Acknowledgements

The work was partially supported by grants-in-aid for Scientific Research (B) (24350112) from the Japan Society for the Promotion of Science (JSPS) and for Scientific Research on Innovative Areas (New Polymeric Materials Based on Element Blocks) (25102504). The work was also supported by the Network Joint Research Center for Materials and Devices and the Nano-Macro Materials, Devices and System Research Alliance (MEXT). The Central Analytical Facility of IMRAM is also acknowledged for allowing us the use of AFM instruments.

Notes and references

1 Y. J. Park, S. J. Kang, B. Lotz, M. Brinkmann, A. Thierry, K. J. Kim and C. Park, *Macromolecules*, 2008, **41**, 8648–8654.
2 S. Ducharme, T. J. Reece, C. M. Othon and R. K. Rannow, *IEEE Trans. Device Mater. Reliab.*, 2005, **5**, 720–735.
3 Z. J. Hu, M. W. Tian, B. Nysten and A. M. Jonas, *Nat. Mater.*, 2009, **8**, 62–67.
4 S. J. Kang, Y. J. Park, I. Bae, K. J. Kim, H. C. Kim, S. Bauer, E. L. Thomas and C. Park, *Adv. Funct. Mater.*, 2009, **19**, 2812–2818.
5 Y. J. Park, I. S. Bae, S. J. Kang, J. Chang and C. Park, *IEEE Trans. Dielectr. Electr. Insul.*, 2010, **17**, 1135–1163.
6 P. Heremans, G. H. Gelinck, R. Muller, K. J. Baeg, D. Y. Kim and Y. Y. Noh, *Chem. Mater.*, 2011, **23**, 341–358.
7 S. J. Kang, I. Bae, Y. J. Shin, Y. J. Park, J. Huh, S. M. Park, H. C. Kim and C. Park, *Nano Lett.*, 2011, **11**, 138–144.
8 Z. Zhang, Q. Meng and T. C. M. Chung, *Polymer*, 2009, **50**, 707–715.
9 A. J. Lovinger, *Macromolecules*, 1981, **14**, 322–325.
10 A. J. Lovinger, *Macromolecules*, 1982, **15**, 40–44.
11 A. J. Lovinger, *Science*, 1983, **220**, 1115–1121.
12 R. Gregorio and R. C. Capitão, *J. Mater. Sci.*, 2000, **35**, 299–306.
13 M. Li, H. J. Wondergem, M.-J. Spijkman, K. Asadi, I. Katsouras, P. W. M. Blom and D. M. de Leeuw, *Nat. Mater.*, 2013, **12**, 433–438.
14 F. Xia, H. S. Xu, F. Fang, B. Razavi, Z. Y. Cheng, Y. Lu, B. M. Xu and Q. M. Zhang, *Appl. Phys. Lett.*, 2001, **78**, 1122–1124.
15 S. Palto, L. Blinov, A. Bune, E. Dubovik, V. Fridkin, N. Petukhova, K. Verkhovskaya and S. Yudin, *Ferroelectr., Lett. Sect.*, 1995, **19**, 65–68.
16 A. V. Bune, V. M. Fridkin, S. Ducharme, L. M. Blinov, S. P. Palto, A. V. Sorokin, S. G. Yudin and A. Zlatkin, *Nature*, 1998, **391**, 874–877.
17 L. M. Blinov, V. M. Fridkin, S. P. Palto, A. V. Bune, P. A. Dowben and S. Ducharme, *Usp. Fiz. Nauk*, 2000, **170**, 247–262.
18 M. Poulsen and S. Ducharme, *IEEE Trans. Dielectr. Electr. Insul.*, 2010, **17**, 1028–1035.
19 S. T. Chen, X. Li, K. Yao, F. E. H. Tay, A. Kumar and K. Y. Zeng, *Polymer*, 2012, **53**, 1404–1408.
20 H. Zhu, M. Mitsuishi and T. Miyashita, *Macromolecules*, 2012, **45**, 9076–9084.
21 H. Zhu, S. Yamamoto, J. Matsui, T. Miyashita and M. Mitsuishi, *J. Mater. Chem. C*, 2014, **2**, 6727–6731.
22 P. Dynarowicz-Latka and K. Kita, *Adv. Colloid Interface Sci.*, 1999, **79**, 1–17.
23 B. Li, Y. Wu, M. Liu and A. R. Esker, *Langmuir*, 2006, **22**, 4902–4905.
24 E. Y. Tsymbal and H. Kohlstedt, *Science*, 2006, **313**, 181–183.
25 A. Bottino, G. Capannelli, S. Munari and A. Turturro, *J. Polym. Sci., Part B: Polym. Phys.*, 1988, **26**, 785–794.
26 A. Salimi and A. A. Yousefi, *J. Polym. Sci., Part B: Polym. Phys.*, 2004, **42**, 3487–3495.
27 T. Miyashita, *Prog. Polym. Sci.*, 1993, **18**, 263–294.
28 T. Miyashita, Y. Mizuta and M. Matsuda, *Br. Polym. J.*, 1990, **22**, 327–331.
29 W. Ou-Yang, M. Weis, X. Y. Chen, T. Manaka and M. Iwamoto, *J. Chem. Phys.*, 2009, **131**, 104702.
30 F. Monroy, F. Ortega and R. G. Rubio, *Phys. Rev. E: Stat. Phys., Plasmas, Fluids, Relat. Interdiscip. Top.*, 1998, **58**, 7629–7641.
31 H. M. Hilles, F. Ortega, R. G. Rubio and F. Monroy, *Phys. Rev. Lett.*, 2004, **92**, 255503.
32 D. L. Thomas, L. J. Blum and A. P. Girard-Egrot, *Biosens. Bioelectron.*, 2005, **20**, 1539–1548.
33 L. Benedini, M. L. Fanani, B. Maggio, N. Wilke, P. Messina, S. Palma and P. Schulz, *Langmuir*, 2011, **27**, 10914–10919.
34 M. Mitsuishi, J. Matsui and T. Miyashita, *Polym. J.*, 2006, **38**, 877–896.
35 M. M. Conde, O. Conde, J. M. Trillo and J. Minones, *Langmuir*, 2011, **27**, 3424–3435.
36 D. T. Balogh, A. Dhanabalan, P. Dynarowicz-Latka, A. Schenning, O. N. Oliveira, E. W. Meijer and R. A. J. Janssen, *Langmuir*, 2001, **17**, 3281–3285.
37 D. López-Díaz and M. M. Velázqueza, *Eur. Phys. J. E*, 2008, **26**, 417–425.
38 B. Martín-García, M. M. Velázquez, J. A. Pérez-Hernández and J. Hernández-Toro, *Langmuir*, 2010, **26**, 14556–14562.
39 A. C. Kucuk, J. Matsui and T. Miyashita, *J. Colloid Interface Sci.*, 2011, **355**, 106–114.
40 D. Risovic, S. Frka and Z. Kozarac, *J. Chem. Phys.*, 2011, **134**, 024701.

41 Y. Seo, K. Paeng and S. Park, *Macromolecules*, 2001, **34**, 8735–8744.
42 M. Mitsuishi, F. Zhao, Y. Kim, A. Watanabe and T. Miyashita, *Chem. Mater.*, 2008, **20**, 4310–4316.
43 I. S. Elashmawi and N. A. Hakeem, *Polym. Eng. Sci.*, 2008, **48**, 895–901.
44 S. Chen, K. Yao, F. E. H. Tay and C. L. Liow, *J. Appl. Phys.*, 2007, **102**, 104108.
45 D. A. Myrzakozha, T. Hasegawa, J. Nishijo, T. Imae and Y. Ozaki, *Langmuir*, 1999, **15**, 3595–3600.
46 M. R. Anderson, M. N. Evaniak and M. Zhang, *Langmuir*, 1996, **12**, 2327–2331.
47 J. R. Hottle, J. J. Deng, H. J. Kim, C. E. Farmer-Creely, B. D. Viers and A. R. Esker, *Langmuir*, 2005, **21**, 2250–2259.
48 J. R. Hottle, H. J. Kim, J. J. Deng, C. E. Farmer-Creely, B. A. Viers and A. R. Esker, *Macromolecules*, 2004, **37**, 4900–4908.
49 A. Jagoda, P. Ketikidis, M. Zinn, W. Meier and K. Kita-Tokarczyk, *Langmuir*, 2011, **27**, 10878–10885.
50 J. Matsui, S. Yoshida, T. Mikayama, A. Aoki and T. Miyashita, *Langmuir*, 2005, **21**, 5343–5348.
51 A. Toda, T. Arita and M. Hikosaka, *Polymer*, 2001, **42**, 2223–2233.
52 D. J. Skrovanek, P. C. Painter and M. M. Coleman, *Macromolecules*, 1986, **19**, 699–705.
53 M. Benz and W. B. Euler, *J. Appl. Polym. Sci.*, 2003, **89**, 1093–1100.
54 R. Gregorio, *J. Appl. Polym. Sci.*, 2006, **100**, 3272–3279.
55 Y. J. Shin, S. J. Kang, H. J. Jung, Y. J. Park, I. Bae, D. H. Choi and C. Park, *ACS Appl. Mater. Interfaces*, 2011, **3**, 582–589.
56 J. Buckley, P. Cebe, D. Cherdack, J. Crawford, B. S. Ince, M. Jenkins, J. J. Pan, M. Reveley, N. Washington and N. Wolchover, *Polymer*, 2006, **47**, 2411–2422.
57 K. Tashiro, Y. Itoh, M. Kobayashi and H. Tadokoro, *Macromolecules*, 1985, **18**, 2600–2606.
58 R. Gregorio and M. Cestari, *J. Polym. Sci., Part B: Polym. Phys.*, 1994, **32**, 859–870.
59 R. Song, G. Xia, X. Xing, L. He, Q. Zhao and Z. Ma, *J. Colloid Interface Sci.*, 2013, **401**, 50–57.